Available online at www.sciencedirect.com

ScienceDirect

Journal of Materiomics 1 (2015) 92–105

www.ceramsoc.com/en/

www.journals.elsevier.com/journal-of-materiomics/

Thermoelectric materials: Energy conversion between heat and electricity

Xiao Zhang, Li-Dong Zhao*

School of Materials Science and Engineering, Beihang University, Beijing 100191, China

Received 10 January 2015; revised 19 January 2015; accepted 20 February 2015
Available online 24 April 2015

Abstract

Thermoelectric materials have drawn vast attentions for centuries, because thermoelectric effects enable direct conversion between thermal and electrical energy, thus providing an alternative for power generation and refrigeration. This review summaries the thermoelectric phenomena, applications and parameter relationships. The approaches used for thermoelectric performance enhancement are outlined, including: modifications of electronic band structures and band convergence to enhance Seebeck coefficients; nanostructuring and all-scale hierarchical architecturing to reduce the lattice thermal conductivity. Several promising thermoelectric materials with intrinsically low thermal conductivities are introduced. The low thermal conductivities may arise from large molecular weights, complex crystal structures, liquid like transports or high anharmonicity of chemical bonds. At the end, a discussion of future possible strategies is proposed, aiming at further thermoelectric performance enhancements.

Keywords: Thermoelectric; Electrical conductivity; Seebeck coefficient; Thermal conductivity

1. Introduction

Statistical results show that more than 60% of energy is lost in vain worldwide, most in the form of waste heat. High performance thermoelectric (TE) materials that can directly and reversibly convert heat to electrical energy have thus draw growing attentions of governments and research institutes [1]. Thermoelectric system is an environment-friendly energy conversion technology with the advantages of small size, high reliability, no pollutants and feasibility in a wide temperature range. However, the efficiency of thermoelectric devices is not high enough to rival the Carnot efficiency [2,3]. A dimensionless figure of merit (ZT) is defined as a symbol of the thermoelectric performance, $ZT=(\alpha^2\sigma/\kappa)T$. Conceptually, to obtain a high ZT, both Seebeck coefficient (α) and electrical conductivity (σ) must be large, while thermal conductivity (κ) must be minimized so that the temperature difference producing Seebeck coefficient (α) can be maintained [4,5].

Historically, in 1821, the German scientist Thomas Johann Seebeck (Fig. 1(a)) noticed an interesting experimental result that a compass needle was deflected by a nearby closed cycle jointed by two different metals, with a temperature difference between junctions. This phenomenon is called the Seebeck effect, which can be simply schematized by Fig. 1(b), where an applied temperature difference drives charge carriers in the material (electrons and/or holes) to diffuse from hot side to cold side, resulting in a current flow through the circuit [6]. Fig. 1(c) shows the power generation efficiency as a function of average ZT_{ave}, and the relationship can be given by Refs. [7,8]:

$$\eta_{\mathrm{p}}=\frac{T_{\mathrm{h}}-T_{\mathrm{c}}}{T_{\mathrm{h}}}\left[\frac{\sqrt{1+ZT_{\mathrm{ave}}}-1}{\sqrt{1+ZT_{\mathrm{ave}}}+T_{\mathrm{c}}/T_{\mathrm{h}}}\right] \tag{1}$$

where ZT_{ave} is the average value of both n-type and p-type two legs, the ZT_{ave} per leg is averaged over the temperature dependent ZT curve between T_{h} and T_{c}, T_{h} and T_{c} are the hot and cold ends temperature, respectively [7,8]:

* Corresponding author.
E-mail address: zhaolidong@buaa.edu.cn (L.-D. Zhao).
Peer review under responsibility of The Chinese Ceramic Society.

http://dx.doi.org/10.1016/j.jmat.2015.01.001

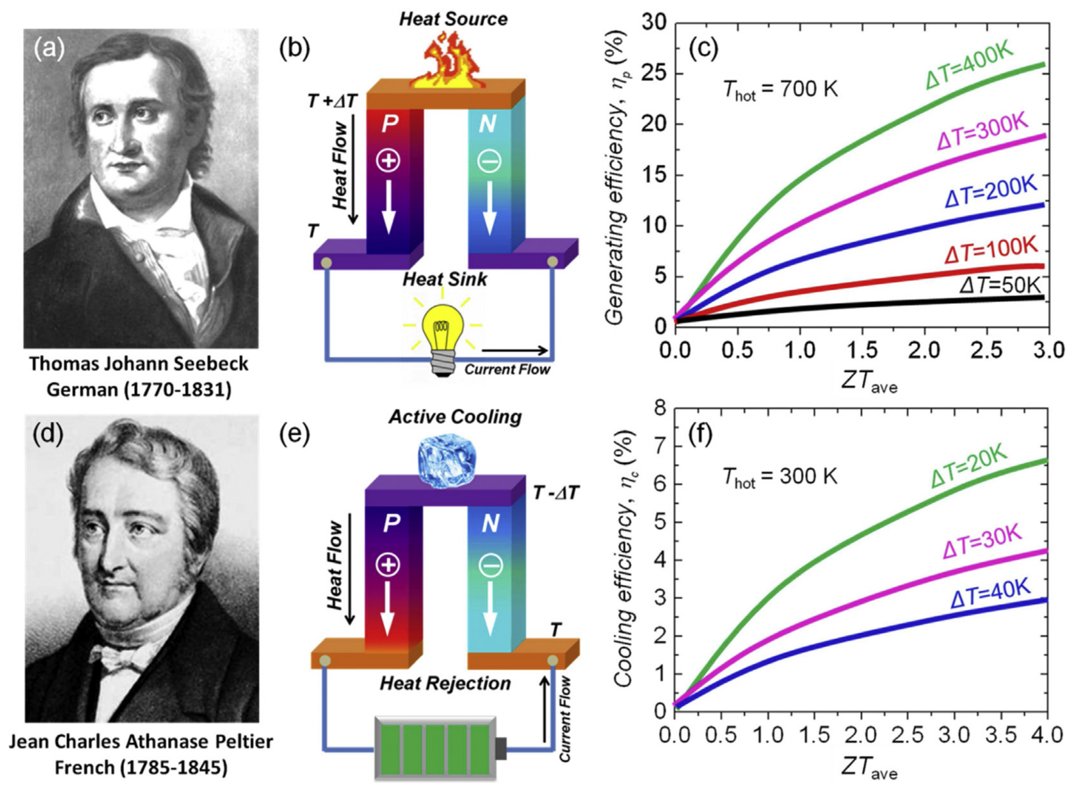

Fig. 1. Schematic illustrations of thermoelectric modules for power generation (Seebeck effect) and active refrigeration (Peltier effect): (a) the German physicist, Thomas Johann Seebeck, (b) Seebeck effect for the power generation, an applied temperature difference causes charge carriers in the material (electrons or holes) to diffuse from the hot side to the cold side, resulting in current flow through the circuit, (c) power generation efficiency as a function of average ZT_{ave}; (d) the French physicist, Jean Charles Athanase Peltier, (e) Peltier effect for the active refrigeration, heat evolves at the upper junction and is absorbed at the lower junction when a current is made to flow through the circuit, (f) cooling efficiency as a function of average ZT_{ave}. Higher ZT_{ave} projects higher thermoelectric power generation and cooling efficiency.

$$ZT_{\mathrm{ave}} = \frac{1}{T_{\mathrm{h}} - T_{\mathrm{c}}} \int_{T_{\mathrm{c}}}^{T_{\mathrm{h}}} ZT\,\mathrm{d}T \tag{2}$$

Fig. 1(c) shows that a higher ZT_{ave} and a larger temperature difference will produce the higher conversion efficiency. One can see that if $ZT_{ave} = 3.0$ and $\Delta T = 400$ K the power generation efficiency η_p can reach 25%, comparable to that of traditional heat engines [7,8]. The Seebeck effect is the thermoelectric power generation model. And in some extreme situations or special occasions, the thermoelectric technology plays an irreplaceable role. The radioisotope thermoelectric generators (RTGs) have long been used as power sources in satellites and space probes, such as Apollo 12, Voyager 1 and Voyager 2, *etc*. Nowadays, thermoelectric power generation gets increasing application in advanced scientific fields, and the thermal source could be fuels, waste-heat, geothermal energy, solar energy and radioisotope [7,8].

Opposite to the Seebeck effect, the Peltier effect is the presence of heating or cooling at an electrified junction of two different conductors and was named after the French physicist Jean Charles Athanase Peltier (Fig. 1(d)), who discovered it in 1834. As shown in Fig. 1(e), heat is absorbed at the upper junction and rejected at the lower junction when a current is made to flow through the circuit, and the upper end is active cooling [6]. The thermoelectric cooling efficiency η_c can be given by Refs. [7,8]:

$$\eta_{\mathrm{c}} = \frac{T_{\mathrm{h}}}{T_{\mathrm{h}} - T_{\mathrm{c}}} \left[\frac{\sqrt{1 + ZT_{\mathrm{ave}}} - T_{\mathrm{h}}/T_{\mathrm{c}}}{\sqrt{1 + ZT_{\mathrm{ave}}} + 1} \right] \tag{3}$$

As illustrated in Fig. 1(f), similar with the thermoelectric power generation, a higher ZT_{ave} value will produce a larger thermoelectric cooling efficiency η_c. For example, When $ZT_{ave} = 3.0$, $\Delta T = 20$ K, η_c could reach 6%. The Peltier effect is the thermoelectric cooling power refrigeration model, which have already been used in some electronic equipments intended for military use. Thermoelectric coolers can also be used to cool computer components to keep temperatures within design limits, or to maintain stable functioning when overclocking. For optical fiber communication applications, where the wavelength of a laser or a component is highly dependent on temperature, Peltier coolers are used along with a thermistor in a feedback loop to maintain a constant temperature and thereby stabilize the wavelength of the device.

2. Current thermoelectric materials and advanced approaches

To obtain a high *ZT*, both Seebeck coefficient (α) and electrical conductivity (σ) must be large, while thermal conductivity (κ) must be minimized; however, the laws of physics conspire against satisfying this requirement. The Wiedemann−Franz law requires the electronic part of thermal conductivity (κ) to be proportional to electrical conductivity (σ), and the Pisarenko relation limits the simultaneous enlargement of α and σ [9]. The complex relationships of these thermoelectric parameters can be summarized as [10]:

$$\alpha = \frac{8\pi^2 k_B^2}{3eh^2} m^* T \left(\frac{\pi}{3n}\right)^{2/3} \tag{4}$$

$$\sigma = ne\mu = \frac{ne^2\tau}{m^*} \tag{5}$$

$$\kappa_{tot} = \kappa_{lat} + \kappa_{ele} = \kappa_{lat} + L\sigma T \tag{6}$$

where k_B is the Boltzmann constant, m^* is the density of states effective mass, h is the Planck constant, n is the carrier concentration, e is per electron charge, μ is the carrier mobility, τ is the relaxation time, κ_{tot} is the total thermal conductivity, κ_{lat} is the lattice thermal conductivity, κ_{ele} is the electronic thermal conductivity, and L is the Lorenz number.

The complex parameter relationships make the approach of tuning carrier concentration alone difficult to enhance *ZT*. However, over the past few decades, great progress has been made in thermoelectric field encompassing diverse strategies to enhance the power factor and reduce thermal conductivity, promoting the thermoelectrics to its *Renaissance* era. Fig. 2 summaries the reported *ZT* values per publishing years. According to the optimal working temperature, the thermoelectric materials can be divided into three ranges [10]: Bi_2Te_3-based low-, PbTe-based middle- and SiGe-based high-temperature ranges, with typical temperatures varying from <400 K, 600 K−900 K and >900 K, respectively. To retrospect the history of thermoelectric materials that have been developed for nearly 200 years since the observation of the Seebeck effect in 1821, the development can be divided into three generations according to *ZT* values [5]. In the first generation, *ZT* is about 1.0, and the devices can operate at a power conversion efficiency 4%−5% (approximately estimated from the maximum *ZT*), as shown in the left purple part of Fig. 2. The second period was ignited by size effects and extends to 1990s [11−13], with *ZT* being pushed to about 1.7 [14], by the introduction of nanostructures; the power conversion efficiency can be expected to be of 11%−15%, as shown in the middle blue part of Fig. 2. The third generation of bulk thermoelectrics has been under development recently, some new concepts and new technologies have pushed *ZT* to 1.8 [15] and even higher; the predicted device conversion efficiency increases to 15%−20%, as shown in the right yellow part of Fig. 2. The development history in the thermoelectric exhibits a trend of pursuing low-cost and earth-abundant characterizations besides high *ZT*s > 2.0 [16−19].

As shown in Fig. 2, due to the extraordinary physical and chemical properties, PbTe is one of the most attractive materials, the study of which was extended throughout the history of thermoelectrics [40−42]. For this reason, PbTe system is hereby chosen to introduce the newly developed strategies in order to enhance *ZT*.

2.1. Band structure engineering to enhance Seebeck coefficient

The first typical example is the Seebeck coefficient enhancement in PbTe by the density-of-states (DOS) distortion through Tl doping [24,43,44]. Such a situation can occur when the valence or conduction band of the host semiconductor resonates with the localized impurity energy level. Compared with Na doped PbTe with the same carrier concentration, Tl

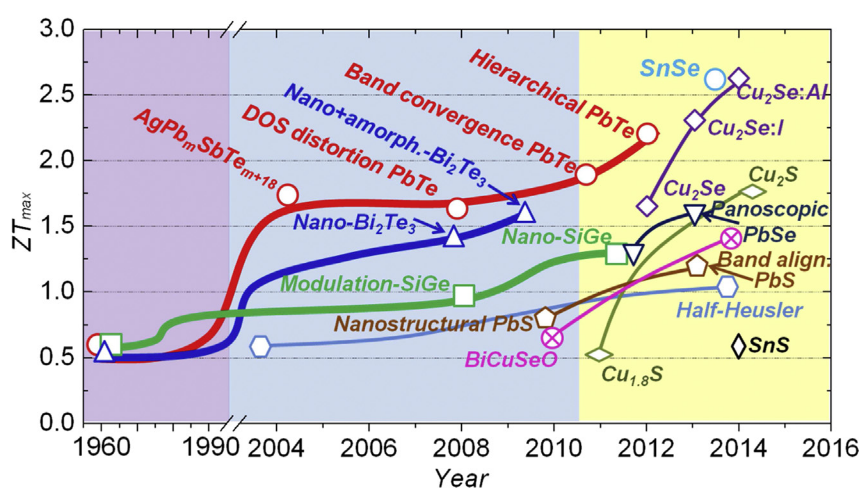

Fig. 2. *ZT* of the current bulk thermoelectric materials as a function of year: the left part indicates the three conventional thermoelectric systems with *ZT* < 1.0 before 1990s, Bi_2Te_3, PbTe and SiGe; the middle part elucidates that the *ZT*s were enhanced to about 1.7 by nanostructures ($AgPb_mSbTe_{m+2}$ [14], nano-Bi_2Te_3 [20], nano+amorphous-Bi_2Te_3 [21], nano-SiGe [22], nanostructural PbS [23]) and electronic structure engineering (Tl doped PbTe [24], $PbTe_{1-x}Se_x$ [15]), modulation doping (SiGe) [25,26]; the right part shows the high performance realized in hierarchical PbTe and promising thermoelectric materials developed recently and characterized by low-cost, earth-abundant, and low thermal conductivity, including panoscopic PbSe [27,28], band alignment PbS [29,30], BiCuSeO [31], Cu_2S systems [32,33], SnS [34,35], Cu_2Se systems [17,19,36,37], Half-Heusler [38,39], and SnSe [18]. Some materials show the *ZT*s > 2.0.

doped PbTe shows increased effective mass and pronuanced higher Seebeck coefficient. The DOS distortion results in a *ZT* as high as 1.5 at 773 K, which is very impressive by merely introducing Tl elements in PbTe. The conjunction of this new physical principle with the approaches used to lower the thermal conductivity could further enhance *ZT* in PbTe system, and have been proved equally applicable in other thermoelectric systems, such as Al-dopd PbSe, such as Al-dopd PbSe [45,46] and In-doped SnTe [47] systems.

Another typical example is the Seebeck coefficient enhancement by tuning the energy offsets between light and heavy valence bands in PbTe. PbTe has a fascinating valence band structure; in addition to the upper light hole band at the *L* points of the highly symmetric Brillouin zone, there exists a second valence (with a heavy effective mass, thus called heavy hole band) band (Σ) which lies energetically below it [5,15,48,49], as shown in Fig. 3(a). The energy offset between *L* and Σ band is about 0.15 eV in PbTe system. If the *L* and Σ band edges move closer in energy the carriers will redistribute between the two valence bands (*L* and Σ bands) with different effect masses. The overall effective mass can be enhanced through carrier injections from Σ band to *L* band by a factor of $N_v^{2/3}$, where N_v is the number of degenerate valleys, which is 4 for *L* band and 12 for the Σ band. Specifically, $m^* = N_v^{2/3} m_b^*$, where m_b^* is the effective mass of the single valley [48]. The band convergence can be evidenced by the deviation of experimental Seebeck coefficients from calculated Pisarenko line at the carrier concentration $> 4 \times 10^{19}$ cm^{-3}, as shown in Fig. 3(b) [50]. Compositional alloying in the matrix could also result in a decreased energy offsets between *L* and Σ bands in PbTe. Examples are Mn [51] and Mg [50] alloyed PbTe, where the energy difference between *L* and Σ bands was reported to decrease with respect to the alloying fractions. With increasing solute fraction of M (M = Mn, Mg), both *L* and Σ bands lower their energies, but the *L* band decreases faster than the Σ band, so that the two bands eventually get closer, Fig. 3(a). This type of M solid solution alloying lifts the Seebeck coefficients over Pisarenko line in the entire carrier concentrations range, Fig. 3(b). The Seebeck coefficient enhancement is similar in character to that caused by resonant states in PbTe by Tl doping. Indeed, the Mn and Mg alloying in PbTe produced a high *ZT* of 1.6 [51] at 700 K and 2.0 [50] at 873 K, respectively. However, this approach is challenged by the deteriorations of carrier mobility, clearly which will need to be settled with future experimentation. The intra matrix band engineering described above has also been successfully applied to other systems such as the PbSe−SrSe [52], Mg_2Si−Mg_2Sn [53] and the SnTe systems [47,54].

2.2. All-scale hierarchical architectures to reduce thermal conductivity

The thermoelectric performance can be enhanced by decreasing the thermal conductivity. The complex relationships between thermoelectric parameters indicate that the lattice thermal conductivity κ_{lat} is the only parameter that is independent on carrier concentration. Therefore, reducing lattice thermal conductivity is an effective method to enhance thermoelectric performance. The lattice thermal conductivity can be given by: $\kappa_{lat} = 1/3 C_v v l$, where the heat capacity (C_v) and the phonon velocity (v) are constant, so the lattice thermal conductivity is governed by the phonon mean free path (MFP) l. When the dimension of inclusions/defects is comparable to the MFP, the phonons will be effectively scattered. Acoustic phonons carry most of the heat in a material, and they have a spectrum of wavelengths and mean free paths (MFP) distribution, including short, medium and long wavelength phonons, synergetically contributes to the total thermal conductivity [56−58]. Therefore, all length-scale structures (solid-solution point defects, nano-scale precipitates and grain boundary) corresponding to the broad spectrum of heat-carrying phonons should be the main design principle for the future thermoelectric materials, as shown in Fig. 4(a).

Point defects can be formed by doping or alloying. Their role of reducing the lattice thermal conductivity [59] are generally understood in the Callaway model *via* the mass difference (mass fluctuations) and the size and the interatomic coupling force differences (strain field fluctuations) between

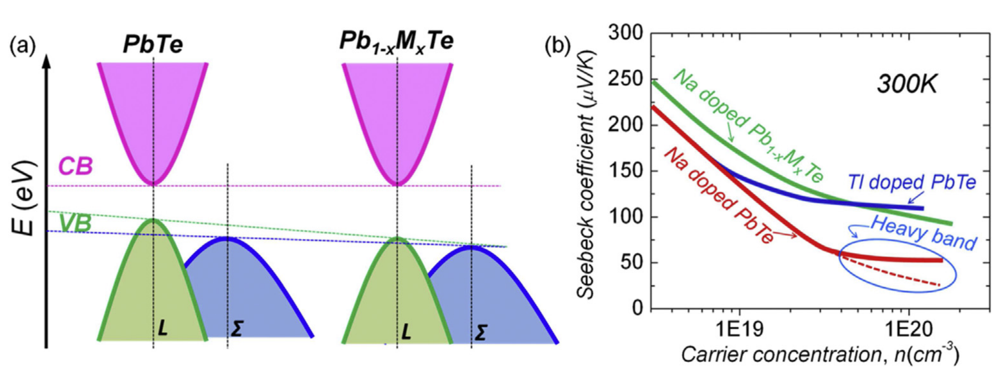

Fig. 3. (a) Schematic showing the relative energy of the valence bands in PbTe system, with rising solid solution fraction *M* (such as Mg [50,55] and Mn [51]). The solid solution alloying within the solubility limit modifies the valence band structure push both *L* and Σ bands move down but make the two valence bands closer in energy. (b) The Pisarenko relation for PbTe (Na doped PbTe), and the enhancement on Seebeck coefficient at a similar Hall carrier concentration in PbTe due to either resonant doping (Tl) [24] or band convergence at room temperature (Mg [50,55] and Mn [51]).

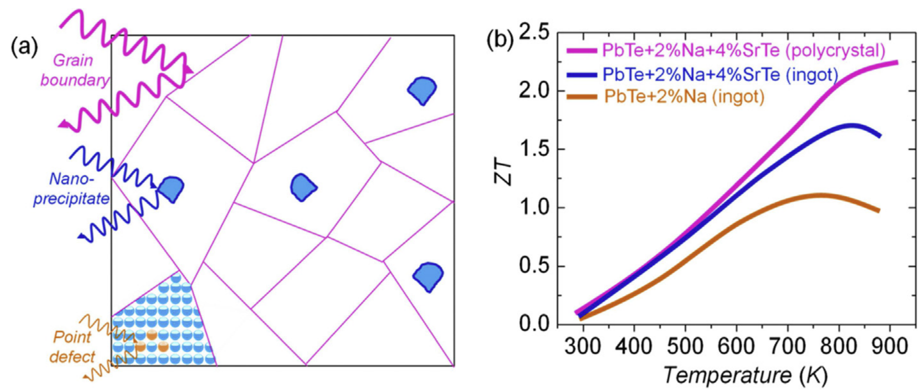

Fig. 4. All-scale hierarchical architectures and *ZT* values: (a) hierarchical architectures with all length-scale structures (solid-solution point defects, nano-scale precipitates and grain boundaries) to scatter short, medium and long wavelength phonons, respectively, (b) the *ZT* values as a function of temperature for the PbTe+2%Na ingot, PbTe+2%Na+4%SrTe ingot, and PbTe+2%Na+4%SrTe polycrystal [16].

the impurity atom and the host lattice [60,61]. Nano-inclusions can be obtained by several approaches, including embedded nano-inclusions [62,63], dispersing *in situ* partially oxidized nanoparticles in matrix [64], and the endotaxial nano-precipitates [23,27,29,50,54,65,66]. A general approach for introducing endotaxial nanostructures in a parent matrix is through nucleation and growth of a second phase, which is required to have a low solubility in the solid state, but complete solubility in the liquid state [23]. To get the polycrystallines, the spark plasma sintering (SPS) is a suitable and effective technology to fabricate highly dense and fine-grained thermoelectric materials [67]. In term of developing scalable materials, there are several effective methods of powder processing, including mechanical alloying (MA) [20,62,68], a rapid melt spinning (MS) [21,69−73], and self-propagating high-temperature synthesis (SHS) [74,75].

An illustrative example for the thermal conductivity reduction is PbTe+2%Na+4%SrTe polycrystalline [16]. The lattice thermal conductivity of PbTe was reduced by ~25% through Na doping; and further reduced by 55% through introducing of nanostructured SrTe; grain boundary contributes to a further significant reduction at high temperatures. The overall thermal conductivity reached as low as ~0.5 W/mK at 915 K. In term of figure of merit *ZT*, optimal Na doping in *p*-type PbTe leaded to a *ZT* of ~1.1 at 775 K, which was further increased to ~1.7 at 800 K by introducing SrTe nano-precipitates, and eventually to ~2.2 at 915 K for PbTe+2%Na+4%SrTe polycrystalline through additional grain

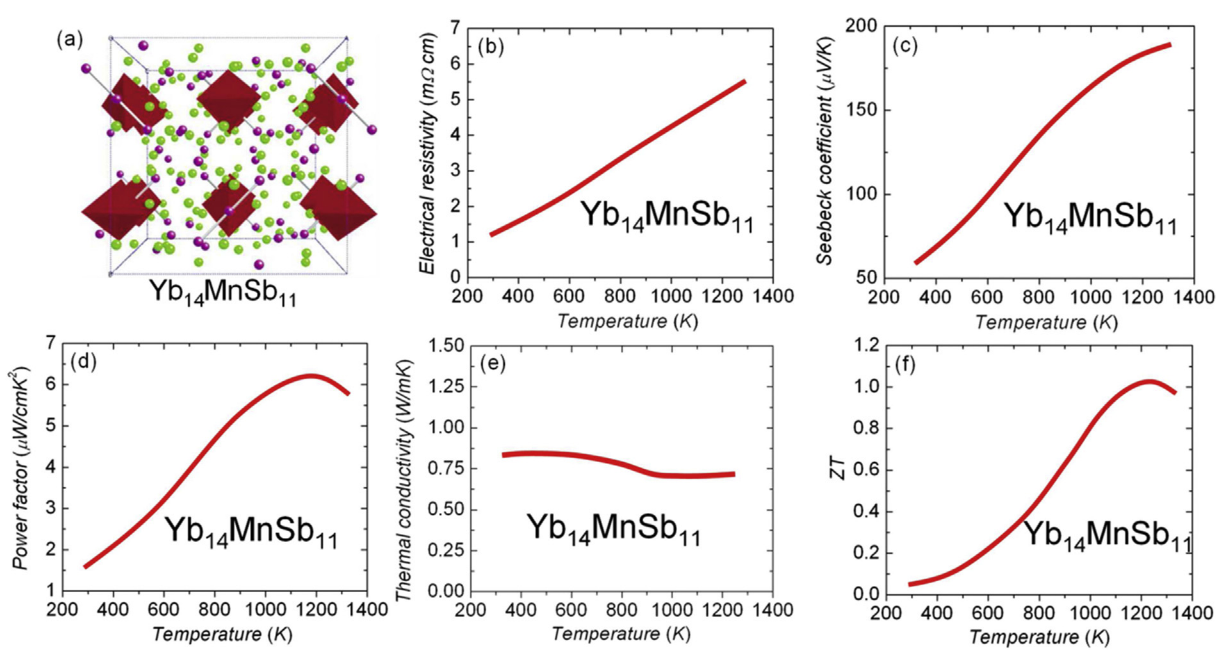

Fig. 5. Crystal structure, and thermoelectric properties as a function of temperature of $Yb_{14}MnSb_{11}$ [77]: (a) Crystal structure, body-centered, $I4_1/acd$ crystal structure of $Yb_{14}MnSb_{11}$. The green and purple spheres represent Yb and Sb, respectively. The $MnSb_4$ tetrahedron is shown as a filled red polyhedron. (b) electrical resistivity, (c) Seebeck coefficient, (d) power factor, (e) thermal conductivity, and (f) *ZT* value. Reprinted (Fig. 5(a)) with permission from (Ref. [61]). Copyright 2006, American Chemical Society.

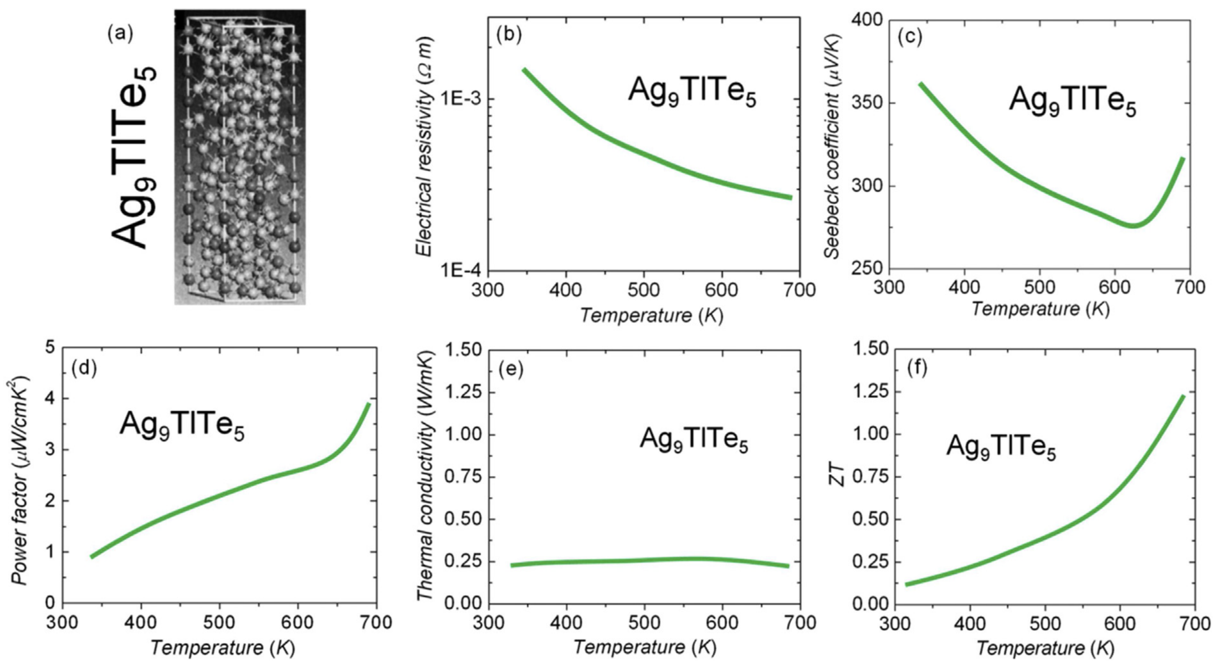

Fig. 6. Crystal structure [78], and thermoelectric properties as a function of temperature of Ag_9TlTe_5: (a) Crystal structure, (b) electrical resistivity, (c) Seebeck coefficient, (d) power factor, (e) thermal conductivity, and (f) *ZT* value. Reprinted (Fig. 6(a)) with permission from (Ref. [62]). Copyright 2005, The American Physical Society.

boundary scattering [16], as shown in Fig. 4(b). These all-scale hierarchical architectures were successfully established and applied to various lead chalcogenides Pb*Q* (*Q* = Te [50], Se [27,65], and S [29,66]).

3. Promising thermoelectric materials with intrinsically low thermal conductivity

To date, diverse advanced approaches to enhance *ZT* emerged in the last decade including: modifying the band structure [24,43], heavy valence (conduction) band convergence [15,53], quantum confinement effects and electron energy barrier filtering to enhance Seebeck coefficients [12,13]; nanostructuring and all-scale hierarchical architecturing to reduce the lattice thermal conductivity [14,16]; band energy alignment between nano-precipitate/matrix to maintain hole mobility [29,76]. Most of these approaches aim to maintain a high power factor and/or reduce the lattice thermal conductivities. Alternatively, one can seek high performance in thermoelectric materials with intrinsically low thermal conductivity, which may arise from a large molecular weight [77], a complex crystal structure [78], anharmonic [18,79,80], anisotropic bonding [59,81], weak chemical bonding [82], or ion liquid-like transport behavior [36,37], *etc*.

3.1. $Yb_{14}MnSb_{11}$: large molecular weight

$Yb_{14}MnSb_{11}$ has a body-centered, $I4_1/acd$ crystal structure, as shown in Fig. 5(a). The green and purple spheres represent Yb and Sb, respectively, and the filled red polyhedron indicates $MnSb_4$ tetrahedron [77]. The molecular weight of $Yb_{14}MnSb_{11}$ is 3783.088, which is more than ten times higher than that of PbTe (334.8). The electrical resistivity (Fig. 5(b)) increases linearly with temperature and reaches ~5.4 × 10^{-3} Ω·cm at 1200 K. The high electrical resistivity corresponds to a low mobility of about 3 cm^2/Vs that decreases with temperature. The Seebeck coefficient for $Yb_{14}MnSb_{11}$ (Fig. 5(c)) reveals a monotonic increase with temperature and reaches a maximum of +185 μV/K at 1275 K. The resulting power factor calculated from the electronic properties exhibits a maximum of ~6.0 μW/cmK^2 at 1200 K, as shown in Fig. 5(d). This value is somewhat low compared with the-state-of-the-art thermoelectric materials [83]. As shown in Fig. 5(e), the thermal conductivity of $Yb_{14}MnSb_{11}$ is very low, ranging from ~ 0.7 to 0.9 W/mK from 300 to 1275 K. The low thermal conductivity value is even comparable to a glass, largely owing to the complexity (limiting the phonon mean-free path) and heavy atomic mass (reducing the fraction of atomic vibrational modes that carry heat efficiently) of the crystal. Overall, the *ZT* for $Yb_{14}MnSb_{11}$ (Fig. 5(f)) sharply increases with temperature and reaches a maximum of ~1.0 at 1223 K. Considering the low power factor of $Yb_{14}MnSb_{11}$, further improvement of the *ZT* should be possible through carrier concentration optimization [84–86].

3.2. Ag_9TlTe_5: a complex crystal structure

As shown in Fig. 6(a), Ag_9TlTe_5 exhibits a complex hexagonal crystal structure with the space group *R*-3 *c*. The hexagonal lattice parameters *a* = 1.1431 nm and *c* = 4.1945 nm. The unit cell of Ag_9TlTe_5 is large and extremely complex, containing 12 molecules and 180 atoms [78]. The electrical resistivity of Ag_9TlTe_5 decreases with temperature across the

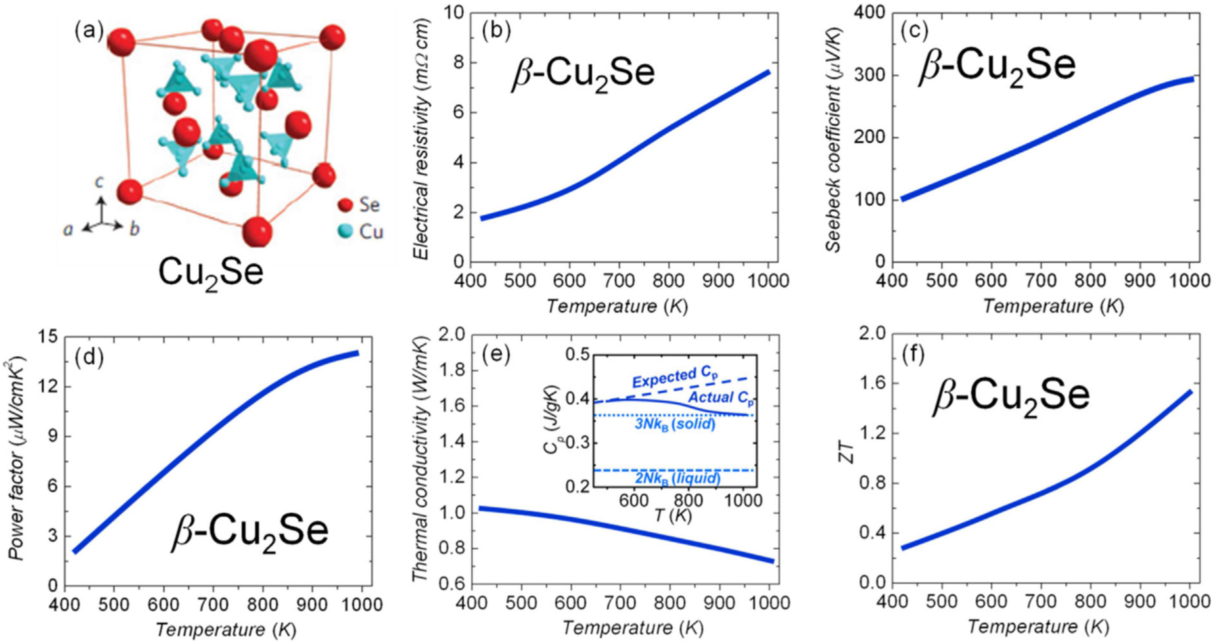

Fig. 7. Crystal structure, and thermoelectric properties as a function of temperature of Cu_2Se: (a) Crystal structure of Cu_2Se at high temperatures (β-phase) with a cubic anti-fluorite structure, the unit cell where only the 8 c and 32f interstitial positions are shown with Cu atoms [37]. (b) electrical resistivity, (c) Seebeck coefficient, (d) power factor, (e) thermal conductivity, and (f) *ZT* value. Inset shows the heat capacity of Cu_2Se as a function of temperature, $3Nk_B$ is the theoretical value (Dulong-Petit) in a solid crystal, $2Nk_B$ is the theoretical value in a liquid, Cu_2Se shows a decreasing and deviating value from the expected C_p at elevating temperature. Reprinted (Fig. 7(a)) with permission from (Ref. [29]). Copyright 2012, Nature Publishing Group.

whole temperature range, indicating a semiconducting character. The resistivity value at 700 K is 2.63×10^{-2} Ω-cm, Fig. 6(b), which is more than an order of magnitude higher than those of state-of-the-art thermoelectric materials. The Seebeck

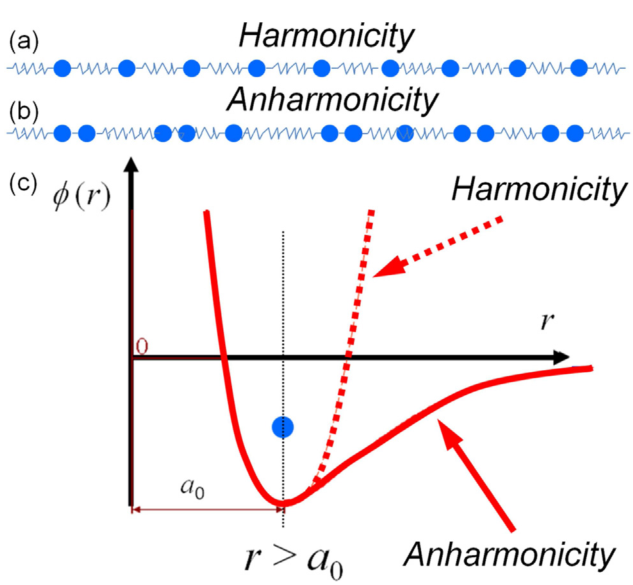

Fig. 8. The schematic representations of harmonicity (a) and anharmonicity (b), the harmonicity shows a balance phonon transport and the anharmonicity shows an imbalance phonon transport (c). Harmonicity: if an atom is pulled from its equilibrium position during the passage of a phonon, the force that the atom is subjected to is proportional to its displacement, and the proportionality constant of this relationship is called the spring constant. Anharmonicity: the spring constant does not remain constant with atom displacements, which has important consequences when two phonons run into each other [88].

coefficient first decreases with temperature, reaching a minimum at around 650 K, and then increases with temperature up to 700 K. The Seebeck coefficient value of Ag_9TlTe_5 at 700 K is 319 μV/K, as shown in Fig. 6(c). The maximum power factor of 3.87 $\mu W/cmK^2$ was obtained at 700 K, Fig. 6(d). Although its power factor is lower than those of state-of-the-art thermoelectric materials, Ag_9TlTe_5 exhibits a very high *ZT* value of 1.23 (Fig. 6(f)) at 700 K because of its extremely low thermal conductivity [78], whose value at room temperature is about 0.23 W/mK, only one-fifth of that for pure Bi_2Te_3 [83]. The temperature dependence of thermal conductivity is rather weak, as shown in Fig. 6(e), resembling a glass-like limit. To explore the reason behind the low thermal conductivity of Ag_9TlTe_5, the elastic properties were then characterized. The average sound velocity, Young's modulus, and Debye temperature are 1203 ms^{-1}, 23.4 GPa and 120 K, respectively. These values are very low compared with those of state-of-the-art thermoelectric materials [83]. For example, the Debye temperatures for Bi_2Te_3 and PbTe are 165 K and 160 K, respectively. The low Young's modulus and Debye temperature of Ag_9TlTe_5 are attributable to its weak interatomic bonding. The above data well satisfied the requirements for a low thermal conductivity: a large molecular weight, a complex crystal structure, nondirectional bonding, and a large number of different atoms per molecule [87].

3.3. Cu_2Se: ion liquid-like transport

Copper chalcogenides Cu_2Se, in spite of their simple chemical formula, have quite complex atomic arrangements. The Cu–Se system exhibits two distinct phases in the Cu-

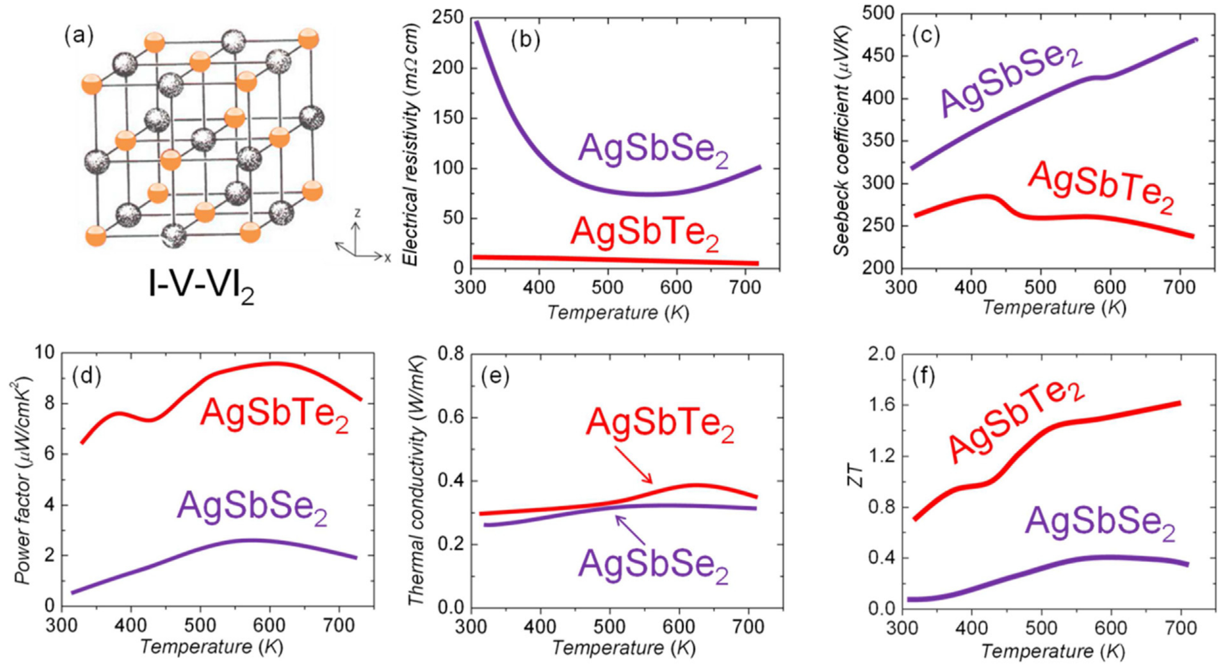

Fig. 9. Crystal structure, and thermoelectric properties as a function of temperature of *I-V-VI*$_2$ semiconductors ($AgSbTe_2$ [79,93] and $AgSbSe_2$ [91,92]): (a) Crystal structure of cubic rock salt I-V-VI_2 semiconductors, yellow atoms present Ag/Sb, gray atoms present Te(Se), (b) electrical resistivities, (c) Seebeck coefficients, (d) power factors, (e) thermal conductivities, and (f) *ZT* values.

deficient region, i.e., the low-temperature α-phase and the high-temperature β-phase. In both phases, a significant deficiency of Cu are allowed in the chemical stoichiometry of Cu_2Se [36,37]. For the high-temperature β-phase, Se atoms form a simple face-centered cubic (*fcc*) structure with the space group *Fm-3 m*, as shown in Fig. 7(a). The electrical resistivity and Seebeck coefficient of Cu_2Se are very high in the whole temperature range, as shown in Fig. 7(b) and (c). The resistivity is on the order of 10^{-2}−10^{-3} Ω-cm, and the Seebeck coefficient in the β-phase range of temperatures from 420 K to 1000 K varies between +80 and +300 μV/K. Based on the measured electrical resistivity and high Seebeck coefficient, the calculated power factor for the β-phase ranges from 7 to 12 μW/cmK^2, as shown in Fig. 7(d). Cu_2Se has very low thermal conductivity values (<1.0 W/mK), see Fig. 7(e); the lattice thermal conductivity κ_{lat} of around 0.4−0.6 W/mK at high temperatures indicates the phonon mean free path is quite small in this binary material. It is very surprising that such low value of κ_{lat} was realized in a compound with very simple chemical formula, small unit cell and light elements. One possible suggestion is that the low thermal conductivity is largely related with the abnormal heat capacity behaviors over temperature, as shown in the inset of Fig. 7(e) β-Cu_2Se shows a decreasing C_p value ranging between $3Nk_B$ (in a solid crystal) and $2Nk_B$ (in a liquid), which deviates from the expected one at elevating temperature. This abnormal behavior of C_p reveals an ion liquid-like transport. With the low thermal conductivity, the *ZT* of β-Cu_2Se reached a value ~ 1.5 at 1000 K, as shown in Fig. 7(f). The extraordinarily high *ZT* of β-Cu_2Se demonstrates that reducing the number of modes of heat propagation by using a superionic conductor with a liquid-like substructure could be a general strategy to suppress lattice thermal conductivity. In this sense, this work indicates a new direction for researches and broadens the scope of materials which should be carefully screened as prospective thermoelectric [68].

3.4. Harmonicity and anharmonicity

The perfectly harmonic bonds in one-dimension are schematically illustrated in Fig. 8(a). In perfectly harmonic bonds, the force to which an atom is subjected is proportional to its displacement from equilibrium position, and the proportionality constant is called the spring constant or stiffness. In the anharmonic case, the spring stiffness does not remain constant with increasing atom displacements, which has pronounced consequences when two phonons run into each other [88], as shown in Fig. 8(b). The presence of the first phonon then changes the value of the spring constant seen by the second phonon. The second phonon thus runs into a medium with modified elastic properties, which is more likely to reflect it. Anharmonicity results in enhanced phonon−phonon scattering, which reduces κ_{lat} without affecting the solid's electronic properties. Grüneisen parameter γ is used to measure the strength of anharmonicity, which can be given by Ref. [79]:

$$\gamma = \frac{3\beta B V_m}{C_v} \quad (7)$$

where β is the volume thermal expansion coefficient, *B* the isothermal bulk modulus, C_v the isochoric specific heat per mole, and V_m the molar volume.

The larger is the Grüneisen parameter γ, the stronger is the phonon scattering. As mentioned above, PbTe system has the extraordinary physical and chemical properties favorable for high thermoelectric performance, one of which is the large Grüneisen parameter γ. PbTe owns a Grüneisen parameter γ about 1.5 [79], which is impressive for a semiconductor. The large γ can be ascribed to the recent discovery that Pb atoms are in fact somewhat displaced off the octahedron center in the rock-salt structure, and that the displacement increases with rising temperature [89]. PbSe shows a lower thermal conductivity than PbTe, since it owns a higher γ value due to a higher C_v. The higher degree of anharmonicity in lattice vibration eventually leads to a lower thermal conductivity in PbSe [90]. In what follows, we would introduce several representative systems with high bonds anharmonicity.

3.4.1. I-V-VI_2 semiconductors

Fig. 9(a) shows the crystal structure of cubic rock-salt I-V-VI_2 semiconductors [79,91,92], where yellow atoms present Ag/Sb, gray atoms present Te(Se). Both the electrical resistivities and Seebeck coefficients of $AgSbTe_2$ [93] and $AgSbSe_2$ [91] are high in the temperature ranging from 300 K to 700 K, as shown in Fig. 9(b) and (c). $AgSbTe_2$ shows the Seebeck coefficients range from 200 to 250 μV/K while $AgSbSe_2$ exhibits much larger values of 300−500 μV/K. The maximal power factors are 10 μW/cmK^2 and 3 μW/cmK^2 for $AgSbTe_2$ and $AgSbSe_2$, respectively, as shown in Fig. 9(d). The thermal conductivities of the two I-V-VI_2 semiconductors are impressively low and remain a value of about 0.3 W/mK throughout the entire temperature range, Fig. 9(e). The low thermal conductivity values contribute high *ZT* values of 1.6 and 0.4 at 700 K for $AgSbTe_2$ [93] and $AgSbSe_2$ [91], respectively, Fig. 9(f). The low thermal conductivity values come from the strong anharmonicity of their chemical bonds, namely, the Grüneisen parameters γ are 2.05 and 3.5 for $AgSbTe_2$ and $AgSbSe_2$, respectively [92]. The high Gruneisen parameters of *I-V-*VI_2 semiconductors may originate from the presence of lone-pair electrons in the *sp*-hybridized bonding orbitals [94,95]. These non-bonded electron pair of Sb gives rise to electron clouds surrounding the Sb atoms that cause nonlinear repulsive forces which is manifested as bonds anharmonicity [92].

3.4.2. BiCuSeO oxyselenides

BiCuSeO oxyselenides have recently received ever-increasing attentions and have been extensively studied as very promising thermoelectric materials [81]. The *ZT* of BiCuSeO system was significantly increased from 0.5 to 1.4 in the past three years, enable BiCuSeO oxyselenides to become robust candidates for energy conversion applications [31,96]. As shown in Fig. 10(a), BiCuSeO crystallizes in a layered ZrCuSiAs structure, with the tetragonal unit cell $a = b = 3.9273$ Å, $c = 8.9293$ Å, $Z = 2$, and the space group *P4/nmm*. BiCuSeO exhibits a two-dimensional layered structure, composed of alternatively stacking of fluorite-like Bi_2O_2 layers and Cu_2Se_2 layers along *c*-axis [97]. The combination of low electrical conductivity and large Seebeck coefficient produce a moderate power factor of undoped BiCuSeO, as shown in Fig. 10(b), (c) and 10(d). Considering the intrinsically low thermal conductivity of BiCuSeO (Fig. 10(e)), a practical way to enhance *ZT* is to increase its electrical transport properties, *i.e.*, the carrier concentration and carrier mobility [81,98,99]. The modulation doping, widely used in a 2-dimension film devices to increase carrier mobilities, is very promising to improve the thermoelectric performance for compounds with intrinsically low thermal conductivities; indeed, the introduction of modulation doping in BiCuSeO increases its carrier mobility from 2 to 4 cm^2/Vs and decouples the power factor [98]. As shown in Fig. 10(f), the figure of merit *ZT* was increased from 1.1 to 1.4 at 923 K in BiCuSeO system by modulation doping. The modulation approach prompts the carrier redistribution between the regions with contrasting carrier mobilities, thus facilitating the overall electrical transport. The heterostructures of modulation doped sample make charge carriers preferentially transport in the low carrier concentration area, which increases carrier mobility by a factor of two while maintains the similar overall carrier concentration as that in the uniformly doped sample [25,26]. The intrinsically low thermal conductivity of BiCuSeO is the main reason for the promising thermoelectric performance in BiCuSeO system, namely, the thermal conductivities of BiCuSeO remain about 0.3−0.5 W/mK throughout the entire temperature range. The elastic properties indicate a Grüneisen parameter of 1.5 in BiCuSeO system [59], which is impressive for a conductor with moderate electrical transport properties. As in the same V group, Bi owns a larger atom radius than that of Sb, thus it is reasonable to expect that the valence shell and electron clouds surrounding the Bi atoms would be larger than that of Sb [59]. Similarly low lattice thermal conductivity should be observed in the Bi-based compounds, in which the Bi ion formally adopts the trivalent state as Sb in $AgSbTe_2$ [79]. The connection between the nature of the bonding and the Grüneisen parameter (γ) has been explored in detail theoretically by Huang et al., who clearly show the effect of large electron clouds on anharmonicity [100]. In principle, the lone-pair electrons of Bi possibly lead to more asymmetric electron cloud density thus resulting in more strong bond anharmonicity [92].

3.4.3. SnSe single crystals

SnSe adopts a layered orthorhombic crystal structure at room temperature, which can be derived from a three dimensional distortion of the NaCl rock-salt structure [101], as shown in Fig. 11(a). Two-atom-thick SnSe slabs (along the *b-c* plane) with strong Sn−Se in-plane bonding are linked with weaker Sn−Se bonding along the *a*-direction. The structure contains highly distorted $SnSe_7$ coordination polyhedron with three short and four very long Sn−Se bonds and a lone pair of the Sn^{2+} atoms sterically accommodated in between the four long Sn−Se bonds [18]. The two-atom-thick SnSe slabs are corrugated creating a zig-zag accordion-like projection along the *b*-axis. Compared with polycrystalline SnSe [102,103], SnSe single crystals exhibit super-high carrier mobilities,

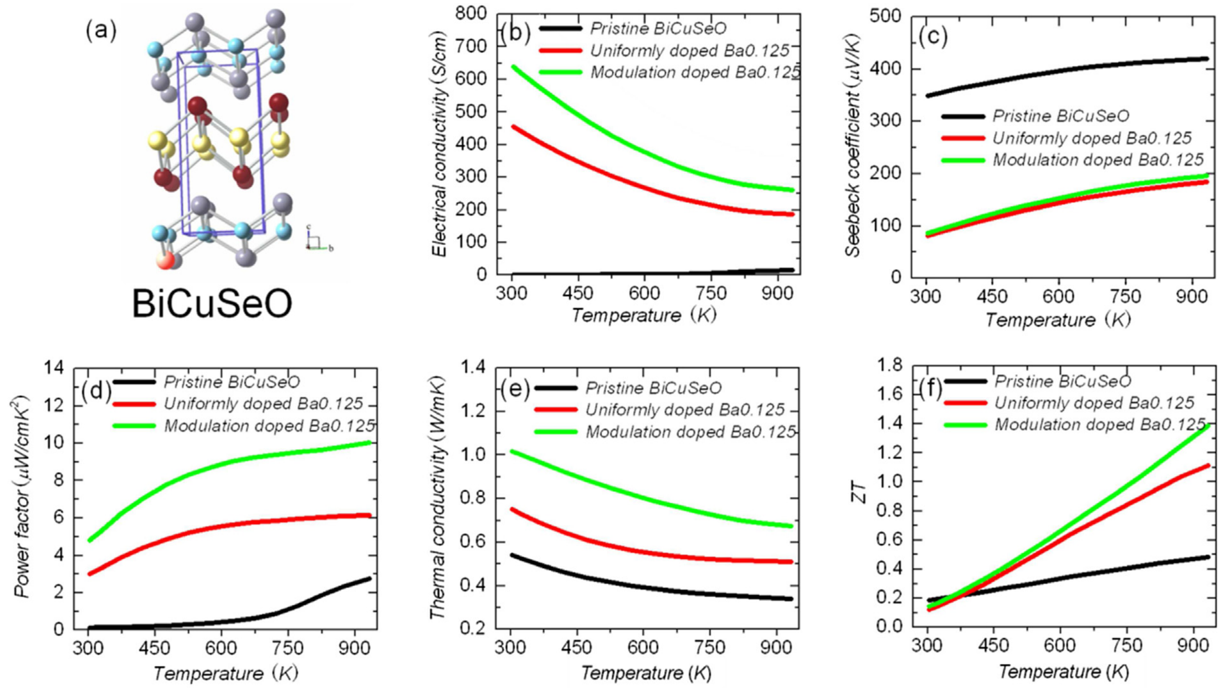

Fig. 10. (a) Crystal structure of BiCuSeO, gray atoms present Bi, blue atoms present O, yellow atoms present Cu, and dark red atoms present Se. Thermoelectric properties as a function of temperature for undoped BiCuSeO, uniformly doped $Bi_{0.875}Ba_{0.125}CuSeO$, and modulation doped $Bi_{0.875}Ba_{0.125}CuSeO$ (50% undoped BiCuSeO + 50% $Bi_{0.75}Ba_{0.25}CuSeO$) [98]: (b) electrical resistivities, (c) Seebeck coefficients, (d) power factors, (e) thermal conductivities, and (f) *ZT* values.

however, the SnSe crystals still show the moderate electrical transport properties, as shown in Fig. 11(b), (c) and (d). Interestingly, SnSe shows a very low thermal conductivity, Fig. 11(e), which is even comparable to these *I-V-VI*$_2$ semiconductors [79]. The physics of SnSe is fascinating, which is due to the high anharmonicity of its chemical bonds. The average Grüneisen parameters of SnSe along the axis of *a*, *b*, *c* are 4.1, 2.1, 2.3, respectively [18]. The anomalously high

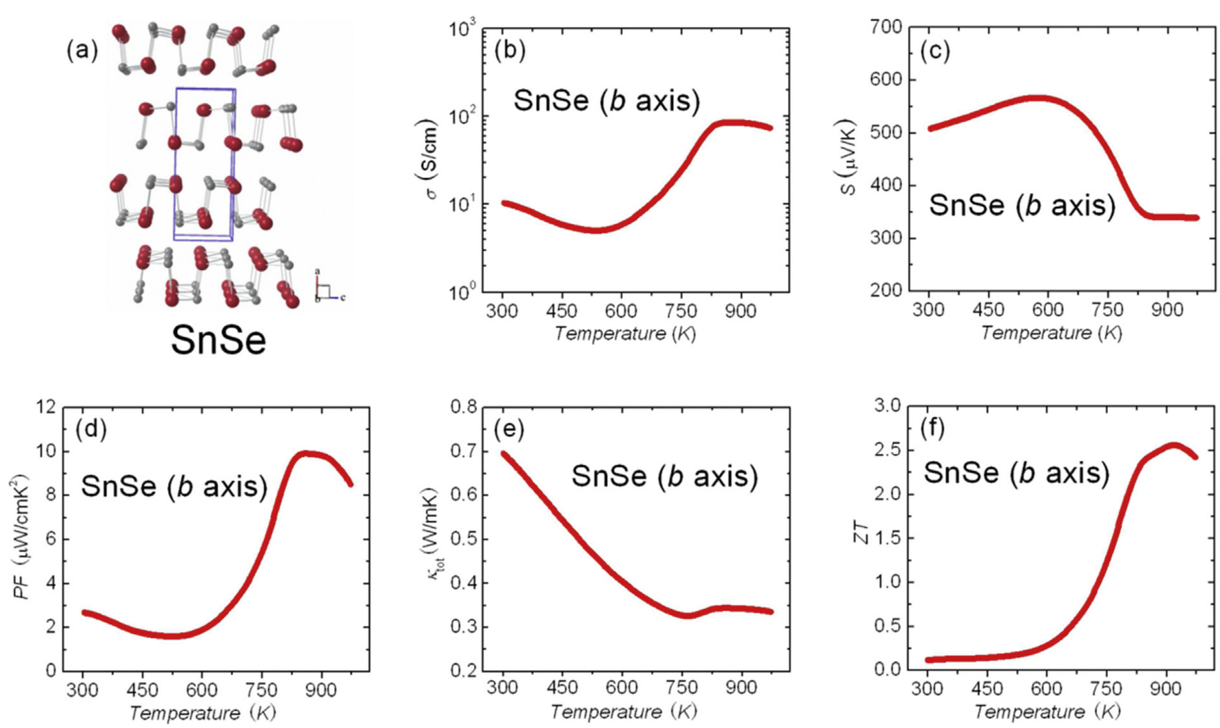

Fig. 11. Crystal structure, and thermoelectric properties as a function of temperature of SnSe single crystal along *b*-axis: (a) Crystal structure of SnSe, gray atoms present Sn, red atoms present Se, (b) electrical resistivity, (c) Seebeck coefficient, (d) power factor, (e) thermal conductivity, and (f) *ZT* value.

Grüneisen parameter of SnSe is a reflection of its unique crystal structure, which contains very distorted $SnSe_7$ polyhedra (due to the lone pair of Sn^{2+}), a zig-zag accordion-like geometry of slabs in the *b-c* plane. In each $SnSe_7$ polyhedra, one Sn atom is surrounded by seven Se atoms, with four long Sn−Se bonds and three short ones, resulting in unbalanced forces around the Sn atom. This implies a soft lattice, and if this lattice were mechanically stressed along the *b* and *c* directions, the Sn−Se bond length would not change directly, but instead the zig-zag geometry would be deformed like a retractable spring or an accordion. In addition, along the *a* direction, the weaker bonding between SnSe slabs provides a good stress buffer or 'cushion', thus dissipating phonon transport laterally. The thermal conductivity of SnSe along *b* axis is 0.70 W/mK at room temperature and decreases to 0.34 W/mK at 973 K (Fig. 11(e)), which results in a high *ZT* of 2.6 at 973 K, Fig. 11(f). Therefore, the high anharmonicity of chemical bonds may well be behind the high *ZT* of SnSe, an idea that stimulates further experimental and theoretical work. As an analog of SnSe, SnS also has been paid extensive attentions. Parker and Singh calculated the band structure of SnS using the first-principles and deduced that SnS is an indirect bandgap semiconductor with a predicted high Seebeck coefficient and a low thermal conductivity [104]. They suggested that *p*-type SnS is a potential thermoelectric material if it can be suitably doped. The newly published calculation work by Bera et al. about SnS also supports the potentially good thermoelectric properties of SnS [105]. Experimentally, Tan et al. reported that the low thermal conductivity falls below 0.5 W/mK at 873 K and leads to a high *ZT* of 0.6 in Ag doped polycrystalline SnS, pointing out that the environmentally friendly SnS is indeed a promising candidate for thermoelectric applications [34].

Owing to the wide scope of promising thermoelectric materials characterized by intrinsically low thermal conductivities, we would not list them one by one in this short summary. Interested readers are encouraged to refer to these typical examples, including CdSb with anisotropic multicenter bonding [106], diamond-like tetrahedral compounds [107−112], natural minerals [113−118], zintl phase with complex structure [119−126], bismuth sulfides [127−133], and others [134−136].

4. Summary and outlook

Thermoelectric materials are environmentally friendly for power generation and refrigeration, thus providing a solution for energy crisis and pollution; however, the thermoelectric conversion efficiency is low and mainly limited by the performance of thermoelectric materials. New concepts and technologies were applied recently to enhance *ZT*, but accompanied difficulties need to be solved. For example, DOS distortion and band convergence could enlarge carrier effective mass and the Seebeck coefficient, but also result in the deterioration of carrier mobility. Nanostructures is an effective approach to reduce the lattice thermal conductivity but also cause a stronger charge carrier scattering. Thermoelectric materials with intrinsically low thermal conductivity deemed promising are facing the problem of poor electrical transport properties. Last but not the least, there is still a long way between high thermoelectric performance and high thermoelectric conversion efficiency. Building a device that could reach the theoretical efficiency is not a trivial pursuit, it is a huge development project by itself considering the tremendous practical challenges, including good thermal isolation of the device, suitable low resistance hot side and cold side metal contacts, and optimizing assembly of modules, *etc*. The development of thermoelectric materials and devices needs the connected efforts involving physicists, chemists, materials scientists, and theory scientists.

Acknowledgments

The work carried out in US was supported in part by a grant DOE-EERE/NSF (CBET-1048728), the Revolutionary Materials for Solid State Energy Conversion, an Energy Frontier Research Center funded by the U.S. Department of Energy, Office of Science, and Office of Basic Energy Sciences under Award Number DE-SC0001054. We thank Professors M. G. Kanatzidis, V. P. Dravid, C. Uher, C. Wolverton, D. N. Seidman, T. P. Hogan, J. P. Heremans, E. D. Case, N. Dragoe, D. Berardan, C.-W. Nan, J.-F. Li, Y. H. Lin, J. Q. He, W. Cai, J. H. Sui, Y. L. Pei, E. Amzallag, Y. Liu, and W. Xu for plentiful discussions and fruitful collaborations. This work was also supported by the "Zhuoyue" program of Beihang University. Of course most of all, we are grateful to the numerous dedicated graduate students and postdoctoral fellows who have contributed to our thermoelectric research efforts. Their names appear in the various publications cited in this article.

References

[1] Kanatzidis MG. Nanostructured thermoelectrics: the new paradigm? Chem Mater 2010;22:648−59.
[2] LaLonde AD, Pei YZ, Wang H, Snyder GJ. Lead telluride alloy thermoelectrics. Mater Today 2011;14:526−32.
[3] Sootsman JR, Chung DY, Kanatzidis MG. New and old concepts in thermoelectric materials. Angew Chem Int Ed 2009;48:8616−39.
[4] He JQ, Kanatzidis MG, Dravid VP. High performance bulk thermoelectrics via a panoscopic approach. Mater Today 2013;16:166−76.
[5] Zhao LD, Dravid VP, Kanatzidis MG. The panoscopic approach to high performance thermoelectrics. Energy Environ Sci 2014;7:251−68.
[6] Li JF, Liu WS, Zhao LD, Zhou M. High-performance nanostructured thermoelectric materials. Npg Asia Mater 2010;2:152−8.
[7] Yang JH. Special section papers on thermoelectric materials and applications − foreword. J Electron Mater 2007;36:703.
[8] Yang JH, Caillat T. Thermoelectric materials for space and automotive power generation. Mrs Bull 2006;31:224−9.
[9] Dresselhaus M. Overview of thermoelectrics for thermal to electrical energy conversion. In: Linke H, Borgstrom M, Pullerits T, Samuelson L, Sundstrom V, Inganas O, editors. Nobel symposium 153: nanoscale energy converters; 2013. p. 36−9.
[10] Snyder GJ, Toberer ES. Complex thermoelectric materials. Nat Mater 2008;7:105−14.
[11] Heremans JP, Dresselhaus MS, Bell LE, Morelli DT. When thermoelectrics reached the nanoscale. Nat Nanotechnol 2013;8:471−3.
[12] Hicks LD, Dresselhaus MS. Effect of quantum-well structures on the thermoelectric figure of merit. Phys Rev B 1993;47:12727−31.

[13] Hicks LD, Dresselhaus MS. Thermoelectric figure of merit of a one-dimensional conductor. Phys Rev B 1993;47:16631−4.

[14] Hsu KF, Loo S, Guo F, Chen W, Dyck JS, Uher C, et al. Cubic $AgPb_mSbTe_{2+m}$: bulk thermoelectric materials with high figure of merit. Science 2004;303:818−21.

[15] Pei YZ, Shi XY, LaLonde A, Wang H, Chen LD, Snyder GJ. Convergence of electronic bands for high performance bulk thermoelectrics. Nature 2011;473:66−9.

[16] Biswas K, He JQ, Blum ID, Wu CI, Hogan TP, Seidman DN, et al. High-performance bulk thermoelectrics with all-scale hierarchical architectures. Nature 2012;489:414−8.

[17] Liu HL, Yuan X, Lu P, Shi X, Xu FF, He Y, et al. Ultrahigh thermoelectric performance by electron and phonon critical scattering in $Cu_2Se_{1-x}I_x$. Adv Mater 2013;25:6607−12.

[18] Zhao LD, Lo SH, Zhang YS, Sun H, Tan GJ, Uher C, et al. Ultralow thermal conductivity and high thermoelectric figure of merit in SnSe crystals. Nature 2014;508:373.

[19] Zhong B, Zhang Y, Li WQ, Chen ZR, Cui JY, Li W, et al. High superionic conduction arising from aligned large lamellae and large figure of merit in bulk $Cu_{1.94}Al_{0.02}Se$. Appl Phys Lett 2014;105.

[20] Poudel B, Hao Q, Ma Y, Lan YC, Minnich A, Yu B, et al. High-thermoelectric performance of nanostructured bismuth antimony telluride bulk alloys. Science 2008;320:634−8.

[21] Xie WJ, Tang XF, Yan YG, Zhang QJ, Tritt TM. Unique nanostructures and enhanced thermoelectric performance of melt-spun BiSbTe alloys. Appl Phys Lett 2009;94.

[22] Bathula S, Jayasimhadri M, Singh N, Srivastava AK, Pulikkotil J, Dhar A, et al. Enhanced thermoelectric figure-of-merit in spark plasma sintered nanostructured n-type SiGe alloys. Appl Phys Lett 2012;101.

[23] Zhao LD, Lo SH, He JQ, Li H, Biswas K, Androulakis J, et al. High performance thermoelectrics from earth-abundant materials: enhanced figure of merit in PbS by second phase nanostructures. J Am Chem Soc 2011;133:20476−87.

[24] Heremans JP, Jovovic V, Toberer ES, Saramat A, Kurosaki K, Charoenphakdee A, et al. Enhancement of thermoelectric efficiency in PbTe by distortion of the electronic density of states. Science 2008;321:554−7.

[25] Zebarjadi M, Joshi G, Zhu GH, Yu B, Minnich A, Lan YC, et al. Power factor enhancement by modulation doping in bulk nanocomposites. Nano Lett 2011;11:2225−30.

[26] Yu B, Zebarjadi M, Wang H, Lukas K, Wang HZ, Wang DZ, et al. Enhancement of thermoelectric properties by modulation-doping in silicon germanium alloy nanocomposites. Nano Lett 2012;12: 2077−82.

[27] Zhao LD, Hao SQ, Lo SH, Wu CI, Zhou XY, Lee Y, et al. High thermoelectric performance via hierarchical compositionally alloyed nanostructures. J Am Chem Soc 2013;135:7364−70.

[28] Wang H, Pei YZ, LaLonde AD, Snyder GJ. Weak electron-phonon coupling contributing to high thermoelectric performance in n-type PbSe. Proc Natl Acad Sci U S A 2012;109:9705−9.

[29] Zhao LD, He JQ, Hao SQ, Wu CI, Hogan TP, Wolverton C, et al. Raising the thermoelectric performance of p-type PbS with endotaxial nanostructuring and valence-band offset engineering using CdS and ZnS. J Am Chem Soc 2012;134:16327−36.

[30] Wang H, Schechtel E, Pei YZ, Snyder GJ. High thermoelectric efficiency of n-type PbS. Adv Energy Mater 2013;3:488−95.

[31] Zhao LD, He JQ, Berardan D, Lin YH, Li JF, Nan CW, et al. BiCuSeO oxyselenides: new promising thermoelectric materials. Energy Environ Sci 2014;7:2900−24.

[32] He Y, Day T, Zhang TS, Liu HL, Shi X, Chen LD, et al. High thermoelectric performance in non-toxic earth-abundant copper sulfide. Adv Mater 2014;26:3974−8.

[33] Ge ZH, Zhang BP, Chen YX, Yu ZX, Liu Y, Li JF. Synthesis and transport property of $Cu_{1.8}S$ as a promising thermoelectric compound. Chem Commun 2011;47:12697−9.

[34] Tan Q, Zhao LD, Li JF, Wu CF, Wei TR, Xing ZB, et al. Thermoelectrics with earth abundant elements: low thermal conductivity and high thermopower in doped SnS. J Mater Chem A 2014;2:17302−6.

[35] Tan Q, Li JF. Thermoelectric properties of Sn-S bulk materials prepared by mechanical alloying and spark plasma sintering. J Electron Mater 2014;43:2435−9.

[36] Liu HL, Shi X, Xu FF, Zhang LL, Zhang WQ, Chen LD, et al. Copper ion liquid-like thermoelectrics. Nat Mater 2012;11:422−5.

[37] Yu B, Liu WS, Chen S, Wang H, Wang HZ, Chen G, et al. Thermoelectric properties of copper selenide with ordered selenium layer and disordered copper layer. Nano Energy 2012;1:472−8.

[38] Xie HH, Wang H, Fu CG, Liu YT, Snyder GJ, Zhao XB, et al. The intrinsic disorder related alloy scattering in ZrNiSn half-Heusler thermoelectric materials. Sci Rep 2014;4.

[39] Xie HH, Wang H, Pei YZ, Fu CG, Liu XH, Snyder GJ, et al. Beneficial contribution of alloy disorder to electron and phonon transport in half-Heusler thermoelectric materials. Adv Funct Mater 2013;23:5123−30.

[40] Allgaier RS, Houston BB. Hall coefficient behavior and the second valence band in lead telluride. J Appl Phys 1966;37:302−9.

[41] Allgaier RS. Valence bands in lead telluride. J Appl Phys 1961;32:2185−9.

[42] Allgaier RS, Scanlon WW. Mobility of electrons and holes in PbS, PbSe, and PbTe between room temperature and 4.2°K. Phys Rev 1958;111:1029−37.

[43] Heremans JP, Wiendlocha B, Chamoire AM. Resonant levels in bulk thermoelectric semiconductors. Energy Environ Sci 2012;5:5510−30.

[44] Wang H, Charoenphakdee A, Kurosaki K, Yamanaka S, Snyder GJ. Reduction of thermal conductivity in PbTe:Tl by alloying with $TlSbTe_2$. Phys Rev B 2011;83.

[45] Zhang QY, Wang H, Liu WS, Wang HZ, Yu B, Zhang Q, et al. Enhancement of thermoelectric figureof-merit by resonant states of aluminium doping in lead selenide. Energy Environ Sci 2012;5:5246−51.

[46] Zhang QY, Yang SQ, Zhang Q, Chen S, Liu WS, Wang H, et al. Effect of aluminum on the thermoelectric properties of nanostructured PbTe. Nanotechnology 2013;24.

[47] Zhang Q, Liao BL, Lan YC, Lukas K, Liu WS, Esfarjani K, et al. High thermoelectric performance by resonant dopant indium in nanostructured SnTe. Proc Natl Acad Sci U S A 2013;110: 13261−6.

[48] Pei YZ, Wang H, Snyder GJ. Band engineering of thermoelectric materials. Adv Mater 2012;24:6125−35.

[49] Gibbs ZM, Kim H, Wang H, White RL, Drymiotis F, Kaviany M, et al. Temperature dependent band gap in PbX (X = S, Se, Te). Appl Phys Lett 2013;103.

[50] Zhao LD, Wu HJ, Hao SQ, Wu CI, Zhou XY, Biswas K, et al. All-scale hierarchical thermoelectrics: MgTe in PbTe facilitates valence band convergence and suppresses bipolar thermal transport for high performance. Energy Environ Sci 2013;6:3346−55.

[51] Pei YZ, Wang H, Gibbs ZM, LaLonde AD, Snyder GJ. Thermopower enhancement in $Pb_{1-x}Mn_xTe$ alloys and its effect on thermoelectric efficiency. Npg Asia Mater 2012;4.

[52] Wang H, Gibbs ZM, Takagiwa Y, Snyder GJ. Tuning bands of PbSe for better thermoelectric efficiency. Energy Environ Sci 2014;7:804−11.

[53] Liu W, Tan XJ, Yin K, Liu HJ, Tang XF, Shi J, et al. Convergence of conduction bands as a means of enhancing thermoelectric performance of n-type $Mg_2Si_{1-x}Sn_x$ solid solutions. Phys Rev Lett 2012;108.

[54] Tan GJ, Zhao LD, Shi FY, Doak JW, Lo SH, Sun H, et al. High thermoelectric performance of p-type SnTe via a synergistic band engineering and nanostructuring approach. J Am Chem Soc 2014;136:7006−17.

[55] Pei YZ, LaLonde AD, Heinz NA, Shi XY, Iwanaga S, Wang H, et al. Stabilizing the optimal carrier concentration for high thermoelectric efficiency. Adv Mater 2011;23:5674.

[56] Lan YC, Minnich AJ, Chen G, Ren ZF. Enhancement of thermoelectric figure of-merit by a bulk nanostructuring approach. Adv Funct Mater 2010;20:357−76.

[57] Minnich AJ, Dresselhaus MS, Ren ZF, Chen G. Bulk nanostructured thermoelectric materials: current research and future prospects. Energy Environ Sci 2009;2:466−79.

[58] Zebarjadi M, Esfarjani K, Dresselhaus MS, Ren ZF, Chen G. Perspectives on thermoelectrics: from fundamentals to device applications. Energy Environ Sci 2012;5:5147−62.
[59] Pei YL, He JQ, Li JF, Li F, Liu QJ, Pan W, et al. High thermoelectric performance of oxyselenides: intrinsically low thermal conductivity of Ca-doped BiCuSeO. Npg Asia Mater 2013;5:e47.
[60] Hu LP, Zhu TJ, Liu XH, Zhao XB. Point defect engineering of high-performance bismuth-telluride-based thermoelectric materials. Adv Funct Mater 2014;24:5211−8.
[61] Jiang GY, He J, Zhu TJ, Fu CG, Liu XH, Hu LP, et al. High performance $Mg_2(Si,Sn)$ solid solutions: a point defect chemistry approach to enhancing thermoelectric properties. Adv Funct Mater 2014;24:3776−81.
[62] Zhao LD, Zhang BP, Li JF, Zhou M, Liu WS, Liu J. Thermoelectric and mechanical properties of nano-SiC-dispersed Bi_2Te_3 fabricated by mechanical alloying and spark plasma sintering. J Alloy Compd 2008;455:259−64.
[63] Xiong Z, Chen XH, Zhao XY, Bai SQ, Huang XY, Chen LD. Effects of nano-TiO_2 dispersion on the thermoelectric properties of filled-skutterudite $Ba_{0.22}Co_4Sb_{12}$. Solid State Sci 2009;11:1612−6.
[64] Zhao XY, Shi X, Chen LD, Zhang WQ, Bai SQ, Pei YZ, et al. Synthesis of YbyCo4Sb12/Yb2O3 composites and their thermoelectric properties. Appl Phys Lett 2006;89.
[65] Lee Y, Lo SH, Androulakis J, Wu CI, Zhao LD, Chung DY, et al. High-performance tellurium-free thermoelectrics: all-scale hierarchical structuring of p-type PbSe-MSe systems (M = Ca, Sr, Ba). J Am Chem Soc 2013;135:5152−60.
[66] Zhao LD, He JQ, Wu CI, Hogan TP, Zhou XY, Uher C, et al. Thermoelectrics with earth abundant elements: high performance p-type PbS nanostructured with SrS and CaS. J Am Chem Soc 2012;134:7902−12.
[67] Noguchi T, Ieee. Powder processing of thermoelectric materials - focusing on SiGe with new sintering technique. 1997.
[68] Li JF, Liu J. Effect of nano-SiC dispersion on thermoelectric properties of Bi_2Te_3 polycrystals. Phys Status Solidi A Appl Mater Sci 2006;203:3768−73.
[69] Zhu TJ, Zhao XB, Hu SH. Phase transition of $FeSi_2$ and Fe_2Si_5 based alloys prepared by melt spinning. J Mater Sci Lett 2001;20:1831−3.
[70] Li H, Tang XF, Su XL, Zhang QJ. Preparation and thermoelectric properties of high-performance Sb additional $Yb_{0.2}Co_4Sb_{12+y}$ bulk materials with nanostructure. Appl Phys Lett 2008;92.
[71] Tan GJ, Liu W, Wang SY, Yan YG, Li H, Tang XF, et al. Rapid preparation of $CeFe_4Sb_{12}$ skutterudite by melt spinning: rich nanostructures and high thermoelectric performance. J Mater Chem A 2013;1:12657−68.
[72] Tan GJ, Zheng Y, Tang XF. High thermoelectric performance of nonequilibrium synthesized $CeFe_4Sb_{12}$ composite with multi-scaled nanostructures. Appl Phys Lett 2013;103.
[73] Tang XF, Xie WJ, Li H, Zhao WY, Zhang QJ, Niino M. Preparation and thermoelectric transport properties of high-performance p-type Bi_2Te_3 with layered nanostructure. Appl Phys Lett 2007;90.
[74] Liang T, Su XL, Yan YG, Zheng G, Zhang Q, Chi H, et al. Ultra-fast synthesis and thermoelectric properties of Te doped skutterudites. J Mater Chem A 2014;2:17914−8.
[75] Su XL, Fu F, Yan YG, Zheng G, Liang T, Zhang Q, et al. Self-propagating high-temperature synthesis for compound thermoelectrics and new criterion for combustion processing. Nat Commun 2014;5.
[76] Biswas K, He JQ, Zhang QC, Wang GY, Uher C, Dravid VP, et al. Strained endotaxial nanostructures with high thermoelectric figure. of merit. Nat Chem 2011;3:160−6.
[77] Brown SR, Kauzlarich SM, Gascoin F, Snyder GJ. $Yb_{14}MnSb_{11}$: new high efficiency thermoelectric material for power generation. Chem Mater 2006;18:1873−7.
[78] Kurosaki K, Kosuga A, Muta H, Uno M, Yamanaka S. Ag_9TITe_5: a high-performance thermoelectric bulk material with extremely low thermal conductivity. Appl Phys Lett 2005;87.
[79] Morelli DT, Jovovic V, Heremans JP. Intrinsically minimal thermal conductivity in cubic I-V-VI(2) semiconductors. Phys Rev Lett 2008;101.
[80] Payne DJ, Egdell RG, Walsh A, Watson GW, Guo J, Glans PA, et al. Electronic origins of structural distortions in post-transition metal oxides: experimental and theoretical evidence for a revision of the lone pair model. Phys Rev Lett 2006;96.
[81] Zhao LD, Berardan D, Pei YL, Byl C, Pinsard-Gaudart L, Dragoe N. $Bi_{1-x}Sr_xCuSeO$ oxyselenides as promising thermoelectric materials. Appl Phys Lett 2010;97.
[82] Chiritescu C, Cahill DG, Nguyen N, Johnson D, Bodapati A, Keblinski P, et al. Ultralow thermal conductivity in disordered, layered WSe_2 crystals. Science 2007;315:351−3.
[83] Rowe DM. CRC handbook of thermoelectrics. CRC Press; 1995.
[84] Cox CA, Brown SR, Snyder GJ, Kauzlarich SM. Effect of Ca doping on the thermoelectric performance of $Yb_{14}MnSb_{11}$. J Electron Mater 2010;39:1373−5.
[85] Mochel A, Sergueev I, Wille HC, Juranyi F, Schober H, Schweika W, et al. Lattice dynamics in the thermoelectric zintl compound $Yb_{14}MnSb_{11}$. Phys Rev B 2011;84.
[86] Yu C, Chen Y, Xie HH, Snyder GJ, Fu CG, Xu JS, et al. Improved thermoelectric properties in Lu-doped $Yb_{14}MnSb_{11}$ zintl compounds. Appl Phys Express 2012;5.
[87] Clarke DR. Materials selection guidelines for low thermal conductivity thermal barrier coatings. Surf Coat Technol 2003;163:67−74.
[88] Heremans JP. The ugly duckling. Nature 2014;508:327−8.
[89] Bozin ES, Malliakas CD, Souvatzis P, Proffen T, Spaldin NA, Kanatzidis MG, et al. Entropically stabilized local dipole formation in lead chalcogenides. Science 2010;330:1660−3.
[90] Wang H, Pei YZ, LaLonde AD, Snyder GJ. Heavily doped p-type PbSe with high thermoelectric performance: an alternative for PbTe. Adv Mater 2011;23:1366−70.
[91] Guin SN, Chatterjee A, Negi DS, Datta R, Biswas K. High thermoelectric performance in tellurium free p-type $AgSbSe_2$. Energy Environ Sci 2013;6:2603−8.
[92] Nielsen MD, Ozolins V, Heremans JP. Lone pair electrons minimize lattice thermal conductivity. Energy Environ Sci 2013;6:570−8.
[93] Wang H, Li JF, Zou MM, Sui T. Synthesis and transport property of $AgSbTe_2$ as a promising thermoelectric compound. Appl Phys Lett 2008;93.
[94] Pan L, Berardan D, Dragoe N. High thermoelectric properties of n-type $AgBiSe_2$. J Am Chem Soc 2013;135:4914−7.
[95] Pei YL, Wu HJ, Sui JH, Li J, Berardan D, Barreteau C, et al. High thermoelectric performance in n-type BiAgSeS due to intrinsically low thermal conductivity. Energy Environ Sci 2013;6:1750−5.
[96] Barreteau C, Pan L, Amzallag E, Zhao LD, Berardan D, Dragoe N. Layered oxychalcogenide in the Bi-Cu-O-Se system as good thermoelectric materials. Semicond Sci Technol 2014;29.
[97] Hiramatsu H, Yanagi H, Kamiya T, Ueda K, Hirano M, Hosono H. Crystal structures, optoelectronic properties, and electronic structures of layered oxychalcogenides MCuOCh (M = Bi, La; Ch = S, Se, Te): effects of electronic configurations of M^{3+} ions. Chem Mater 2008;20:326−34.
[98] Pei YL, Wu HJ, Wu D, Zheng FS, He JQ. High thermoelectric performance realized in a BiCuSeO system by improving carrier mobility through 3D modulation doping. J Am Chem Soc 2014;136:13902−8.
[99] Sui JH, Li J, He JQ, Pei YL, Berardan D, Wu HJ, et al. Texturation boosts the thermoelectric performance of BiCuSeO oxyselenides. Energy Environ Sci 2013;6:2916−20.
[100] Huang BL, Kaviany M. Structural metrics of high-temperature lattice conductivity. J Appl Phys 2006;100.
[101] Baumgardner WJ, Choi JJ, Lim Y-F, Hanrath T. SnSe Nanocrystals: synthesis, structure, optical properties, and surface chemistry. J Am Chem Soc 2010;132:9519−21.
[102] Chen CL, Wang H, Chen YY, Day T, Snyder GJ. Thermoelectric properties of p-type polycrystalline SnSe doped with Ag. J Mater Chem A 2014;2:11171−6.
[103] Sassi S, Candolfi C, Vaney JB, Ohorodniichuk V, Masschelein P, Dauscher A, et al. Assessment of the thermoelectric performance of polycrystalline p-type SnSe. Appl Phys Lett 2014;104.

[104] Parker D, Singh DJ. First principles investigations of the thermoelectric behavior of tin sulfide. J Appl Phys 2010;108.

[105] Bera C, Jacob S, Opahle I, Gunda NSH, Chmielowski R, Dennler G, et al. Integrated computational materials discovery of silver doped tin sulfide as a thermoelectric material. Phys Chem Chem Phys 2014;16:19894–9.

[106] Wang S, Yang J, Wu L, Wei P, Yang J, Zhang W, et al. Anisotropic multicenter bonding and high thermoelectric performance in electron-poor CdSb. Chem Mater 2015;27:1071–81.

[107] Li YL, Zhang TS, Qin YT, Day T, Snyder GJ, Shi X, et al. Thermoelectric transport properties of diamond-like $Cu_{1-x}Fe_{1+x}S_2$ tetrahedral compounds. J Appl Phys 2014;116.

[108] Fan J, Liu HL, Shi XY, Bai SQ, Shi X, Chen LD. Investigation of thermoelectric properties of $Cu_2Ga_xSn_{1-x}Se_3$ diamond-like compounds by hot pressing and spark plasma sintering. Acta Mater 2013;61:4297–304.

[109] Liu RH, Xi LL, Liu HL, Shi X, Zhang WQ, Chen LD. Ternary compound $CuInTe_2$: a promising thermoelectric material with diamond-like structure. Chem Commun 2012;48:3818–20.

[110] Shi XY, Huang FQ, Liu ML, Chen LD. Thermoelectric properties of tetrahedrally bonded wide-gap stannite compounds $Cu_2ZnSn_{1-x}In_xSe_4$. Appl Phys Lett 2009;94.

[111] Shi XY, Xi LL, Fan J, Zhang WQ, Chen LD. Cu-Se bond network and thermoelectric compounds with complex diamondlike structure. Chem Mater 2010;22:6029–31.

[112] Xi L, Zhang YB, Shi XY, Yang J, Shi X, Chen LD, et al. Chemical bonding, conductive network, and thermoelectric performance of the ternary semiconductors Cu_2SnX_3 (X = Se, S) from first principles. Phys Rev B 2012;86.

[113] Qiu PF, Zhang TS, Qiu YT, Shi X, Chen LD. Sulfide bornite thermoelectric material: a natural mineral with ultralow thermal conductivity. Energy Environ Sci 2014;7:4000–6.

[114] Fan XF, Case ED, Lu X, Morelli DT. Room temperature mechanical properties of natural-mineral-based thermoelectrics. J Mater Sci 2013;48:7540–50.

[115] Lu X, Morelli DT. Rapid synthesis of high-performance thermoelectric materials directly from natural mineral tetrahedrite. Mrs Commun 2013;3:129–33.

[116] Lu X, Morelli DT. Natural mineral tetrahedrite as a direct source of thermoelectric materials. Phys Chem Chem Phys 2013;15:5762–6.

[117] Lu X, Morelli DT, Xia Y, Zhou F, Ozolins V, Chi H, et al. High performance thermoelectricity in earth-abundant compounds based on natural Mineral tetrahedrites. Adv Energy Mater 2013;3:342–8.

[118] Li JH, Tan Q, Li JF. Synthesis and property evaluation of $CuFeS_{2-x}$ as earth-abundant and environmentally-friendly thermoelectric materials. J Alloy Compd 2013;551:143–9.

[119] Bux SK, Zevalkink A, Janka O, Uhl D, Kauzlarich S, Snyder JG, et al. Glass-like lattice thermal conductivity and high thermoelectric efficiency in $Yb_9Mn_{4.2}Sb_9$. J Mater Chem A 2014;2:215–20.

[120] Kauzlarich SM, Condron CL, Wassei JK, Ikeda T, Snyder GJ. Structure and high-temperature thermoelectric properties of $SrAl_2Si_2$. J Solid State Chem 2009;182:240–5.

[121] May AF, Toberer ES, Snyder GJ. Transport properties of the layered zintl compound $SrZnSb_2$. J Appl Phys 2009;106.

[122] Prytz O, Flage-Larsen E, Toberer ES, Snyder GJ, Tafto J. Reduction of lattice thermal conductivity from planar faults in the layered zintl compound $SrZnSb_2$. J Appl Phys 2011;109.

[123] Toberer ES, Zevalkink A, Crisosto N, Snyder GJ. The zintl compound $Ca_5Al_2Sb_6$ for low-cost thermoelectric power generation. Adv Funct Mater 2010;20:4375–80.

[124] Zevalkink A, Takagiwa Y, Kitahara K, Kimura K, Snyder GJ. Thermoelectric properties and electronic structure of the zintl phase $Sr_5Al_2Sb_6$. Dalton Trans 2014;43:4720–5.

[125] Zevalkink A, Toberer ES, Zeier WG, Flage-Larsen E, Snyder GJ. Ca_3AlSb_3: an inexpensive, non-toxic thermoelectric material for waste heat recovery. Energy Environ Sci 2011;4:510–8.

[126] Zevalkink A, Zeier WG, Pomrehn G, Schechtel E, Tremel W, Snyder GJ. Thermoelectric properties of Sr_3GaSb_3-a chain-forming zintl compound. Energy Environ Sci 2012;5:9121–8.

[127] Biswas K, Zhao LD, Kanatzidis MG. Tellurium-free thermoelectric: the anisotropic n-type semiconductor Bi_2S_3. Adv Energy Mater 2012;2:634–8.

[128] Du XL, Cai FS, Wang XW. Enhanced thermoelectric performance of chloride doped bismuth sulfide prepared by mechanical alloying and spark plasma sintering. J Alloy Compd 2014;587:6–9.

[129] Ge ZH, Zhang BP, Shang PP, Yu YQ, Chen C, Li JF. Enhancing thermoelectric properties of polycrystalline Bi_2S_3 by Optimizing a Ball-Milling process. J Electron Mater 2011;40:1087–94.

[130] Ge ZH, Zhang BP, Yu ZX, Li JF. Effect of spark plasma sintering temperature on thermoelectric properties of Bi_2S_3 polycrystal. J Mater Res 2011;26:2711–8.

[131] Kim JH, Bilc D, Loo S, Short J, Mahanti SD, Hogan T, et al. Synthesis and thermoelectric properties of $AgBi_3S_5$. In: Nolas GS, Yang J, Hogan TP, Johnson DC, editors. Thermoelectric materials 2003-research and applications; 2004. p. 201–6.

[132] Mrotzek A, Chung DY, Hogan T, Kanatzidis MG. Structure and thermoelectric properties of the new quaternary tin selenide $K_{1-x}Sn_{5-x}Bi1_{1+x}Se_{22}$. J Mater Chem 2000;10:1667–72.

[133] Zhao LD, Zhang BP, Liu WS, Zhang HL, Li JF. Enhanced thermoelectric properties of bismuth sulfide polycrystals prepared by mechanical alloying and spark plasma sintering. J Solid State Chem 2008;181:3278–82.

[134] Pei YL, Zhang CL, Li J, Sui JH. Electrical and thermal transport properties of $AgIn_5Te_8$. J Alloy Compd 2013;566:50–3.

[135] Tyagi K, Gahtori B, Bathula S, Srivastava AK, Shukla AK, Auluck S, et al. Thermoelectric properties of Cu_3SbSe_3 with intrinsically ultralow lattice thermal conductivity. J Mater Chem A 2014;2:15829–35.

[136] Zhang Y, Skoug E, Cain J, Ozolins V, Morelli D, Wolverton C. First-principles description of anomalously low lattice thermal conductivity in thermoelectric Cu-Sb-Se ternary semiconductors. Phys Rev B 2012;85.

Xiao Zhang is a doctoral research fellow in the School of Materials Science and Engineering at Beihang University, China. She received her Bachelor of Engineering degree in metallurgy from the University of Science and Technology Beijing, China, in 2013. She started her doctoral research as a member of Li-Dong Zhao's group in 2014. Her main research interests focus on the fabrication and properties of thermoelectric materials.

Li-Dong Zhao is currently associate professor of Beihang University, China. He received his B.E. and M.E. Degrees in Material Science from the Liaoning Technical University and his Ph.D. Degree in Material Science from the University of Science and Technology Beijing, China in 2009. He was postdoctoral research fellow in the LEMHE-ICMMO (CNRS-UMR 8182) at the University of Paris-Sud from 2009 to 2011, and continued a postdoctoral research fellow in Mercouri G. Kanatzidis group in the Department of Chemistry at the Northwestern University from 2011 to 2014. His research interests include the thermoelectric materials, superconductors and thermal barrier coatings.